Anal. Bioanal. Electrochem., Vol. 15, No. 4, 2023, 264-279
https://www.doi.org/10.22034/abec.2023.704566

Analytical & Bioanalytical Electrochemistry

www.abechem.com

Full Paper

Two-step *vs.* Single-Step Electrochemical Anodizing Process Regarding Anti-Corrosion Properties of Titanium

Lamia Bouchama,[1,2,*] Yazid Bouznit,[3,4] Nawel Boukmouche,[5] and Sarah Irki[6]

[1]*Faculty of Technology, Department of Renewable Energy, Blida 1 University, Soumaa, Blida 09000, Algeria*
[2]*Chemical Engineering Laboratory, Department of Industrial Chemistry, Blida 1 University, Soumaa, Blida 09000, Algeria*
[3]*Laboratory of Materials: Elaboration–Properties–Application, University of Jijel, Jijel 18000, Algeria*
[4]*Faculté des Sciences, Département de chimie, Université de M'Sila, 28000 M'Sila, Algeria*
[5]*Faculty of Technology, Department of Process Engineering, USTHB University, Babezzouar, Alger 16000, Algeria*
[6]*Department of Chemistry Blida 1 University, Soumaa, Blida 09100, Algeria*

*Corresponding Author, Fax: +21325272709
E-Mail: bouchmalamia@yahoo.fr ; lamia.bouchama@univ-blida.dz

Received: 12 January 2023 / Received in revised form: 25 April 2023 / Accepted: 26 April 2023 / Published online: 30 April 2023

Abstract- Two-step anodizing approach is a simple way to produce an adhesive and continuous layer while improving the stability of titanium oxide in aggressive aqueous media. A comparative study of the electrochemical behavior of TiO_2 anodic films formed by single-step (SSA) and two-step (TSA) anodizing processes has been investigated. The anodic films have been characterized by SEM, EDX, GDOES, XRD, and FTIR analysis. Potentiodynamic polarization and EIS were used to investigate corrosion behavior in corrosive environments. A completely different surface morphology of anodic films has been obtained. Surface oxide film thicknesses of specimens were estimated at 51.86 and 60.67 µm for the SSA and TSA processes, respectively. In both cases, X-ray diffraction revealed an amorphous nature. EIS results showed that corrosion performance is closely related to anodic film morphology including thick layers, compactness, uniformity, and stability, as proved by the TSA process. Analysis of dynamic potential polarization confirmed that the TSA approach enhanced corrosion resistance by increasing (E_{corr}) and lowering (I_{corr}). The corrosion potential (Ecorr) increased from -0.309 V/ECS to -0.271 V/ECS for the SSA and TSA and the I_{corr} value decreased from 1.410 µA.cm^{-2} to 1.032 µA.cm^{-2} for SSA and TSA approaches respectively.

Keywords- Anodizing process; Corrosion resistance; EIS; Titania; Two-step anodizing

1. INTRODUCTION

Titanium and titanium-based alloys have excellent physical and chemical properties, namely: excellent strength and lightweight properties; low density; high mechanical properties; cryogenic temperature resistance; corrosion resistance; and biocompatibility, making them attractive candidates for a wide range of industrial applications, such as power engineering, transportation, mining equipment, the chemical industry, the food industry, etc. Titanium-based alloys are also preferred over other alloys for marine applications, such as oil rig pillars, risers, pumps, aquarium exhibit equipment, etc., due to their excellent resistance to both acidic environments and oceans [1-4].

However, frictional components in marine environments typically suffer from tribocorrosion, which is the combined effect of mechanical wear and chemical corrosion [5]. Though, titanium-based alloys' high corrosion resistance in aggressive environments, it is because of the naturally forming titania on their surface, which can have a few nanometers of thickness. Thin titanium films tend to deteriorate in harsh environments, such as seawater. This causes poor tribological performance, which leads to a limited component lifespan and application range and also makes it unable to resolve the necessary requirements [1,2,6].

In this context, additional surface treatment is usually required to improve the superficial mechanical properties: wear resistance, and superficial hardness, as well as the corrosion resistance of titanium alloys [7]. An extremely wide range of surface treatment processes is available, such as laser shock, penning, thermal oxidation, ion implementation, and thermal oxidation. Further, anodizing is the most efficient technique to enhance mechanical properties and corrosion resistance [1]. However, the single-step anodizing technology has certain limitations regarding thickness, color, and microstructure control of the film and hence cannot perfectly satisfy material requirements. More specifically, there is still a lot of room for improvement in corrosion resistance, wear resistance, and biocompatibility [8].

In reality, previous research on the properties of titanium and its alloy traditionally anodized by single-step anodizing revealed poor mechanical and corrosion resistance qualities because of a high number of cracks and structural defects, which are not stable enough for real-life application [9].

A two-step anodizing technique appears appropriate for the development of such ordered porous structures due to its low cost, and relatively straightforward nature, as well as its efficiency if corrosion resistance and mechanical properties are improved in comparison to those achieved on commonly elaborated titania films [10].

On that basis, we propose an improved two-step anodization process for the purpose of improving the corrosion properties of pure titanium up to the level of more expensive alloys frequently used for marine applications, starting with a gradual increase in thickness to achieve a predominantly amorphous phase to achieve the final aim of this study. The

corrosion behavior in hard environments has been investigated using EIS, potentiodynamic polarization, complemented with SEM, EDX, GDOES, XRD, and FTIR analysis.

2. EXPERIMENTAL SECTION

In the present work, commercially pure titanium has been used as the substrate material. To obtain a surface roughness of about R_a:1 µm, all specimens were dry-polished using abrasive paper (grids #120 to #1200). The surface of titanium specimens (60 mm×40 mm×1 mm) was degreased with acetone and electropolished in a mixed solution of perchloric acid and ethanol (1:4 volumes) under a constant voltage of 23 V for 2 min below 5 °C to obtain a smooth surface. In the final step of pretreatment, the specimens were rinsed in ethanol and dried with air. Anodic oxidation of titanium was performed in an electrochemical cell, where the titanium sheets were used as an anode and another as a counter-electrode. Single-step anodization (SSA) of titanium was carried out in potenstiostatic mode (30 V) in a sulfuric acid electrolyte (1 M) for up to 4 hours at 5 °C.

For the two-step anodization (TSA), the titanium oxide formed during the first anodization step was peeled off by ultra-sonically soaking. Then, the newly dimpled Ti substrates were anodized for the second time under the same conditions as SSA.

The crystallinity of the oxide film was determined using XRD on a Panalytical X'Pert PRO diffractometer with CuK radiation (=1.5425). The morphology, chemical composition, and their distribution in anodic films were examined using a Quanta 200 scanning electron microscope (SEM). Chemical analysis and depth profile concentration were investigated by glow discharge optical emission spectroscopy (GDOES) using a GD Profiler. A Shimadzu FTIR-8400S spectrometer in transmission mode was used to investigate the nature of chemical bonding in anodic films.

Voltalab 40 (PGZ301) was used to investigate the electrochemical behavior of the anodic films, using the conventional three-electrode system (a saturated calomel electrode (SCE) as a reference electrode, a pure platinum plate was used as a counter electrode, and the sample with an area of 1 cm^2 as a working electrode). The electrochemical behavior of the samples was measured by EIS at room temperature by applying an AC amplitude of 10 mV to the open-circuit potential over the frequency range from 100 kHz to 1 mHz, with five points per decade. The EIS measurements were performed by immersing the anodized specimens in an unstirred and aerated 3.5 wt.% NaCl solution at different periods of immersion, namely; 2, 8, 24, and 48 h, respectively. Potentiodynamic polarization was conducted after immersion in a 3.5 wt.% NaCl solution for an hour.

3. RESULTS AND DISCUSSION

3.1. Morphological analysis

Figure 1 shows the surface topography images of the samples (SSA and TSA). An obvious difference in porosity and topography on the surface of samples has been seen.

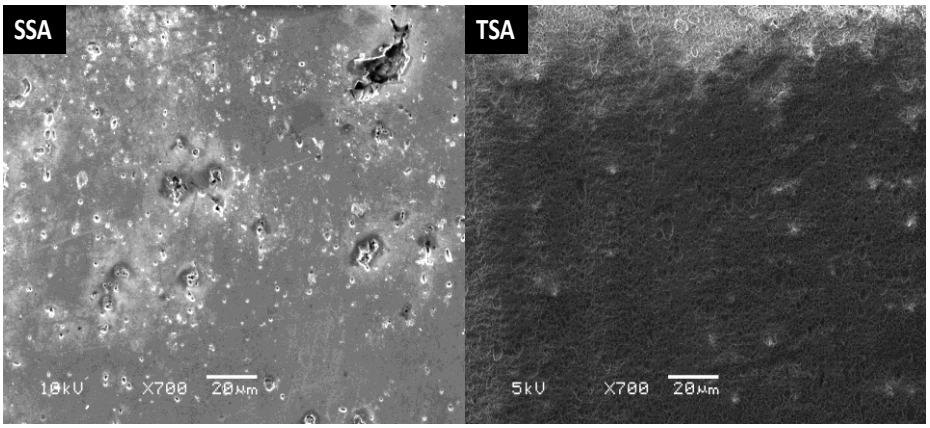

Figure 1. SEM micrographs of the titania anodic films

Examination of the surface morphology of the anodic film generated by SSA revealed the presence of many pores of various shapes and sizes distributed heterogeneously on the surface. In addition, image analysis showed the presence of many cracks of a few microns in length caused by the field-assisted dissolution of the oxide. According to X. Yu et al. [11], dissolution occurs only in preferred locals, resulting in the formation of some microcracks on the surface oxide layer. Because the aqueous solution penetrates microcracks, it dissolves faster than in other areas of the oxide layer. This surface morphology has previously been reported by Z. Wang et al. [11,12]. The same microstructure of titanium oxide film anodized in sulfuric and HF acids have also been described by Al-Radha et al. [13].

In contrast, a covered, compact, thick anodic film structure is formed with the appearance of small nodules on the oxide film surface produced by the TSA process, as seen in Figure 1. This structure is formed by the growth of cells following the imprints produced by dissolving the first layer in phosphoric acid. It can reduce the sample surface porosity by increasing the film density and stability [12]. Lazarouk et al. [14] believe that expelled gases are dissolved in low-temperature electrolytes at the outer surface with the highest gas solubility. In this way, pores are prevented from being periodically blocked by gas bubbles, and the electrochemical process stays continuous. Fuhr et al. observed the same micrographs of titanium anodized in pyroligneous liquor 50% at a current density of 1 $mA.cm^{-2}$ for 600 s [15]. Also, J. Winiarski et al. [16] have observed the same micrograph after anodic polarization of titanium in a DES bath at 30 V for 10 min at 60 °C.

3.2. Elemental analysis

A cross-sectional EDS concentration profile illustrating the compositional analysis of titanium oxide films is shown in Figure 2. It was observed that the films were relatively thick,

at about 51.8 and 59.2 µm for the specimens obtained by the SSA and TSA processes, respectively. It is well known that the oxide thickness increases almost linearly with treatment duration. EDS revealed that the developed films were composed predominantly of O, Ti, and a minor quantity of sulfur, which may be coming from the anodizing electrolyte (H_2SO_4). In sulfuric acid, porous films can be contaminated with acid species (SO_4^{-2}) [17,18].

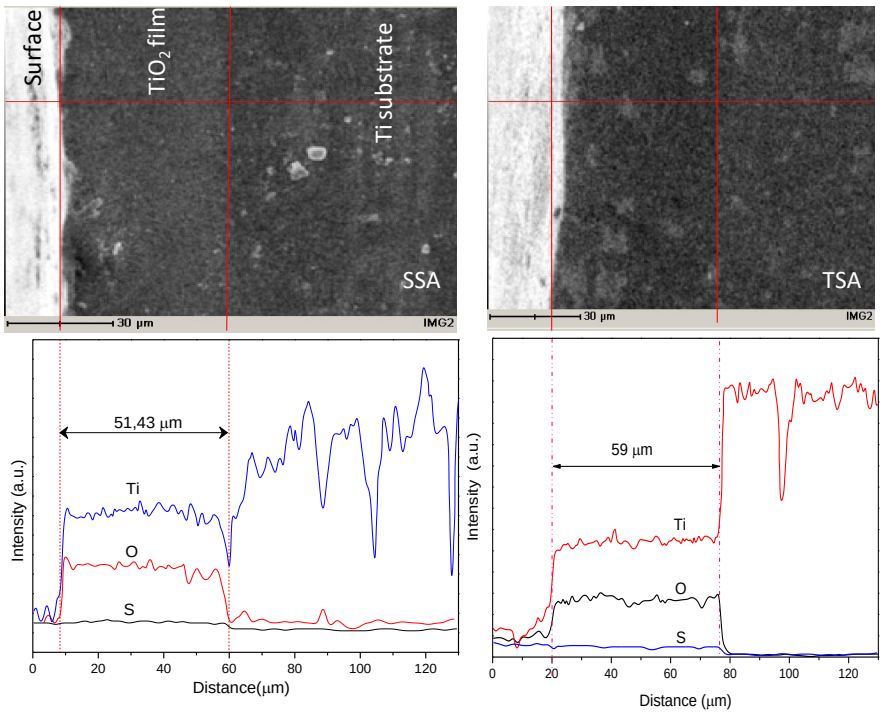

Figure 2. SEM images of a cross-section of the TiO_2 anodic films and EDS concentration profiles of the Ti, O, and S atoms in the TiO_2 anodic film

3.3. Glow discharge optical emission spectrometry (GDOES)

GDOES depth profiling results of anodic films formed by SSA and TSA processes are shown in Figure 3. The curves presented give the element distribution of titania anodic films in weight percentages versus the depth of the anodic films. It can be seen that Ti and O are the main elements composing the anodic films, but S was the minor one, which was considered a contamination that comes from the electrolytic species [19]. It was evident that the sulfur species were incorporated relatively uniformly in the outer regions of the anodic films. GDOES analysis reveals a high oxygen content. This would be logical because it combines with Ti to form TiO_2 and then decreases gradually. According to Wang et al. [12], Ti and O are present in the film with different distributions in the two layers: in the porous layer, they were uniform, while in the barrier layer, Ti increased and O decreased. The thicknesses of oxide films on the surfaces of specimens were estimated to be 51.86 and 60.67 µm for the SSA and TSA processes, respectively. This result shows that the TSA can considerably increase the thickness of the film. On the other hand, Zheng et al. [20] reported

that the Ti anodizing in H_2SO_4 solution led to a higher oxide thickness, owing to the fact that the rate of TiO_2 formation is much higher than that of dissolution. According to Z. Liu et al. [21], anodic films formed in aqueous electrolytes are usually contaminated with species derived from electrolyte anions. They have found the same pace of GDOES elemental depth profiles for anodic oxide films formed on cp-Ti at 100 V (a), 150 V (b), and 200 V (c) in 1 M phosphoric acid for 900 s.

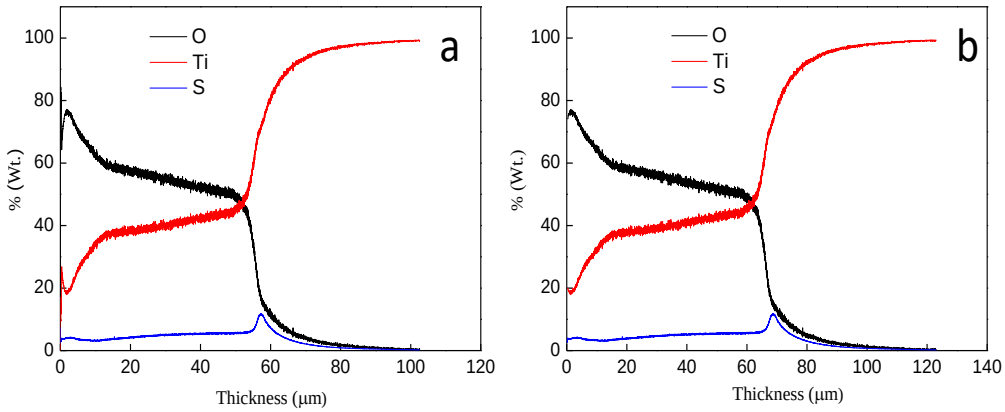

Figure 3. Glow discharge optical emission spectrometry (GDOES) spectra of the anodic layer on titanium films

3.4. Structural analysis

The X-ray diffraction patterns recorded for the samples are shown in Figure 4. The XRD patterns exhibit several peaks at about 2=35.09°, 38.09°, 40.18°, 53.0°, 70.65°, and 77.34° related to the (100), (002), (101), (102), (103), and (201) diffraction planes, which can correspond to the titanium substrate (JCPDS file: 44-1294) reflecting the formation of amorphous Ti oxide. The peak for metallic titanium substrates is because of X-ray penetration into the substrate through the thin nanoporous TiO_2 layers.

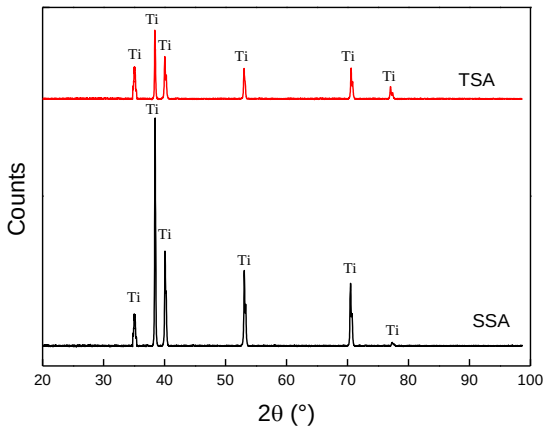

Figure 4. XRD pattern of TiO_2 anodic layers

It is worth noting that, an increase in the time of anodization provides the increased thickness of the TiO_2 layer, reflecting the decreasing intensity of Ti substrates, which peaks in the case of TSA (the thicker film). This conclusion confirms the results obtained by EDX and GDOES analyses. Recent research by V.M. Prida et al. [22] found similar results. They discovered amorphous Ti oxide by anodic oxidation in $HF+H_2SO_4$. M.A. Selimin et al. [23] reported that amorphous Ti oxide was obtained with an anodized sample at 50 V in 0.3 M of H_2SO_4. Similar amorphous phases have been found by K. Indira [24].

3.5. Infrared spectroscopy

Figure 5 illustrates the infrared spectra of titania anodic films formed by SSA (black line) and TSA (red line). As seen in Figure 5, a weak absorption band at 1055 cm^{-1} results from S=O stretching vibrations originating from the electrolytic species (H_2SO_4) [10]. For both samples, the strong and broad peak in the regions of 800–400 cm^{-1}, typically at 564 and 776 cm^{-1}, reflects the Ti–O–Ti stretching vibrations [25,26]. The FTIR results corroborate the findings of the EDX and GDOES analyses.

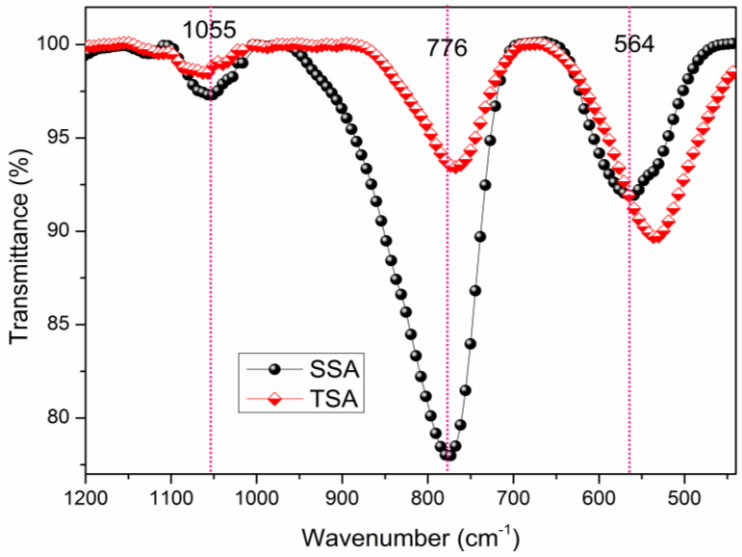

Figure 5. FTIR spectra of the TiO_2 anodic layer formed by (black line) SSA and (red line) TSA

3.6. Corrosion resistance

It is well known that commercially pure titanium may suffer different forms of corrosion in very severe environments. In this context, this study aims to improve the anti-corrosion properties of the anodic titania film treated by the TSA process. The corrosion behavior of the anodic films was investigated using EIS and dynamic potential polarization (Tafel) at 25 °C in a neutral (3.5 wt.% NaCl) aqueous solution.

3.6.1. Impedance spectra of anodic films

In Figure 6, the Nyquist plots show two overlapping capacitive loops. Previous studies have shown that the low-frequency domains are correlated to the inner layer properties, and the high-frequency domain reflects the outer porous layer properties [27,28].

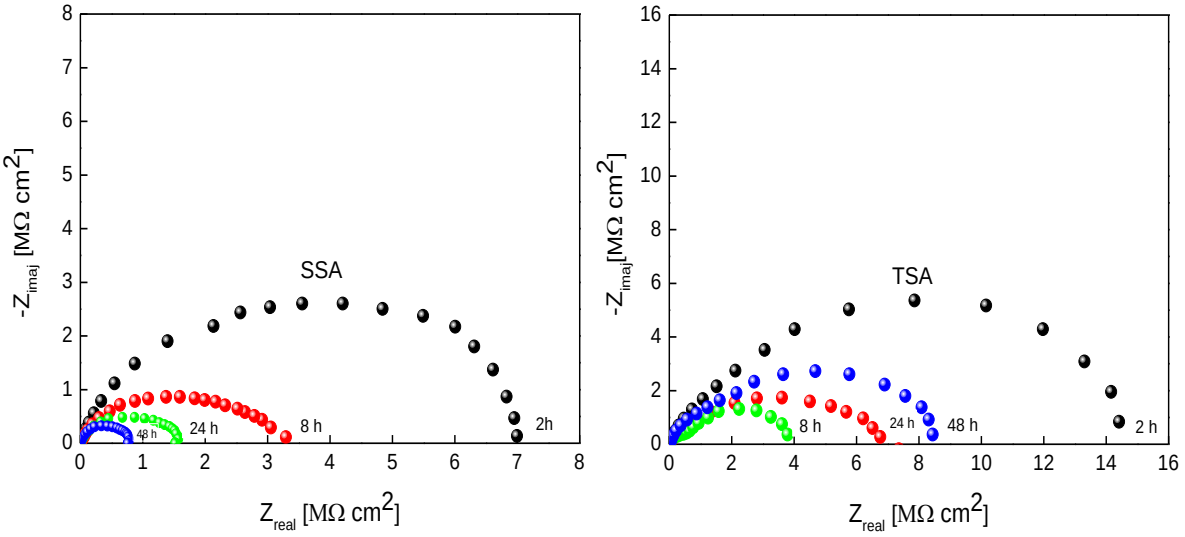

Figure 6. Nyquist plots as a function of immersion time of titania anodic layers in 3.5 wt% NaCl solution at 25 °C

The porous layer responds, probably due to the natural self-sealing in the NaCl solution as reported by some authors [29]. According to Fadl-Allah et al. [17], the impedance values in the low-frequency domain reflect corrosion resistance. The polarization resistance values, which are directly related to corrosion resistance, were derived by fitting the Nyquist plots.

As shown in Fig. 6, the highest corrosion resistance corresponds to the anodized film formed by the TSA process as a result of the thin and compact layers, while the lowest value is recorded for the sample obtained by the SSA process. As seen in Fig. 6, the diameter of the capacitive loop decreases during immersion, reflecting a decrease in corrosion resistance for both specimens. Moreover, for samples treated via TSA, the diameter of the capacitive loop sharply increases at 48 hours, reflecting an increase in polarization resistance.

3.6.1.1. Electrical equivalent circuit

EIS data were analyzed using ZView software by fitting an equivalent circuit model. The proposed equivalent circuit (EC) model is illustrated in Fig. 7. This EC presented the closest fit to the impedance data. A similar CE has been obtained for both SSA and TSA approaches. As shown in SEM images, the only difference between TSA and SSA is the shape of the porous film cells. The TSA presented an ordered cell shape, whereas SSA has an irregular cell shape. This EC model has been used previously to simulate titanium anodic film EIS data

[30]. This model is composed of three parts in series; the first is electrolyte resistance (Rel). The second part was a parallel combination of a constant phase element (CPE_p) and a R_p, which characterized the porous layer's properties. The latter part is a parallel branch of a constant phase element (CPE_b) and a R_b, which characterizes the barrier layer's properties.

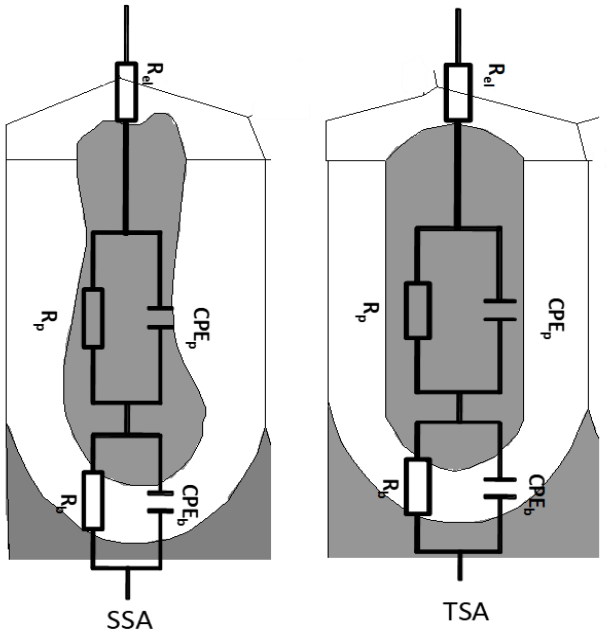

Figure 7. Equivalent circuits (EC) for simulating the behavior of TiO_2 anodic layers

The components of the circuit have the following meanings:

R_{el} represents the resistance of the electrolyte between the surface of the anodic film and the reference electrode. R_{el} is negligible in a NaCl solution.

R_P: the porous layer resistance, which is described by the electrolyte conductivity in the film pores and the film porosity.

CPE_p: constant phase element, accounting for the irregularities, non-ideal capacitance, and variations in the properties of the porous oxide film [30]. The inner layer is characterized by R_b (barrier layer resistance) and CPE_b of the barrier layer. The impedance of a CPE is given by:

$$CPE=1/(2\pi JfC)^{\alpha} \quad (1)$$

where α_p and α_b, due to the non-ideal capacitive behaviors, correspond to CPE_p and CPE_b, respectively [30].

Fitted experimental impedance diagrams are illustrated in Figure 8. Fitted data are represented by red lines, while experimental data are shown in black dots. On the whole, we found that R_b is much higher than R_p for both approaches, SSA and TSA. Accordingly, anodic oxide film resistance strongly depends on the barrier layer. The R_b values for the TSA technique after two hours of immersion in NaCl solution were 10.60 $M\Omega.cm^2$ versus 04.10

MΩ.cm^2 for R_p. However, for the SSA approach, the R_b values are about 04.89 MΩ.cm^2 versus 02.10 MΩ.cm^2 for R_p.

In addition, we notice that the TSA approach provides higher values of R_p and R_b than the SSA approach. After 48 hours of immersion in the NaCl solution, the R_b values for the TSA method are 06.40 MΩ.cm^2 versus 00.59 MΩ.cm^2 for the single method. Similarly, TSA's and SSA's R_p values are about 02.07 MΩ.cm^2 and 00.17 MΩ.cm^2, respectively.

For the single-step anodizing process, R_b and R_P values decrease gradually with immersion time (R_b from 04.89 MΩ.cm^2 at 2 h to 00.59 MΩ.cm^2 at 48 h) and (R_P from 02.10 MΩ.cm^2 at 2 h to 00.17 MΩ.cm^2 at 48 h). There has been significant degradation of the porous and barrier layers due to poor protection of the heterogeneous porous layer. This is due to the electrolyte's ability to penetrate the porous layer to attack the barrier layer.

Nevertheless, for the two-step anodizing process, both R_b and R_p values decrease during the first immersion time (R_b from 10.60 MΩ.cm^2 at 2 h to 02.04 MΩ.cm^2 at 24 h) and (R_p from 04.06 MΩ.cm^2 at 2 h to 01.92 MΩ.cm^2 at 24 h), which is due to the dissolution of the anodic film. After 48 hours, R_b and R_p rise sharply (around 06.40 MΩ.cm^2 and 02.07 MΩ.cm^2, respectively), indicating that the barrier layer has not been attacked. Porous surfaces with high homogeneity and low permeability are more effective at preventing electrolyte penetration, retarding corrosion, and inhibiting barrier layer degradation. As a result, the EIS results are in significant agreement with the SEM analysis results.

The polarization resistance can be calculated using ($R_{pol} = R_{ele} + R_p + R_b$). Moreover, the corrosion resistance of anodized samples in an electrolyte depends on the barrier properties of the oxide film and on the transport of ions and electrons across it [31]. According to Bayat et al., in determining the corrosion resistance of titanium, the oxide thickness, evenness, and compactness are the most important factors in the quality of the oxide film. Samples anodized with SSA have lower corrosion resistance, perhaps as a result of cracks in the oxide layers, which can exist with a thicker oxide film.

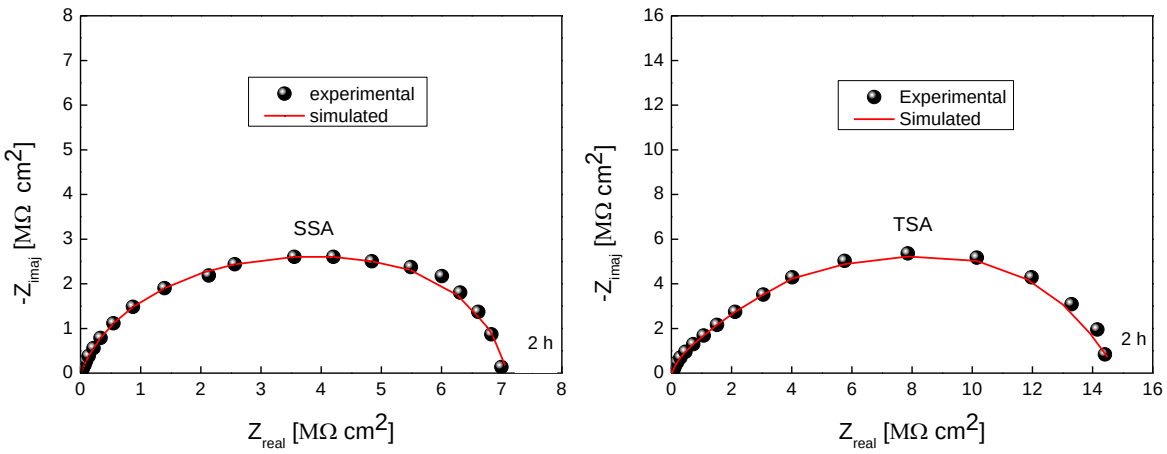

Figure 8. Fitting of the Nyquist plots immersed in 3.5 wt% NaCl solution at 25 °C for 2 h

The variation of polarization resistance (R_p) as a function of immersion time for anodized specimens is shown in Figure 9. At the beginning of immersion, the R_p value for the sample obtained by the SSA process was approximately 6.99 MΩ.cm^2. There has been a noticeable decrease in its value, which indicates the degradation of the anodized film over time, essentially due to the heterogeneous distribution of porosity and cracks present in the outermost porous layer of the anodic film. which allows Cl^- ions to easily penetrate the oxide film, affecting its corrosion resistance [10].

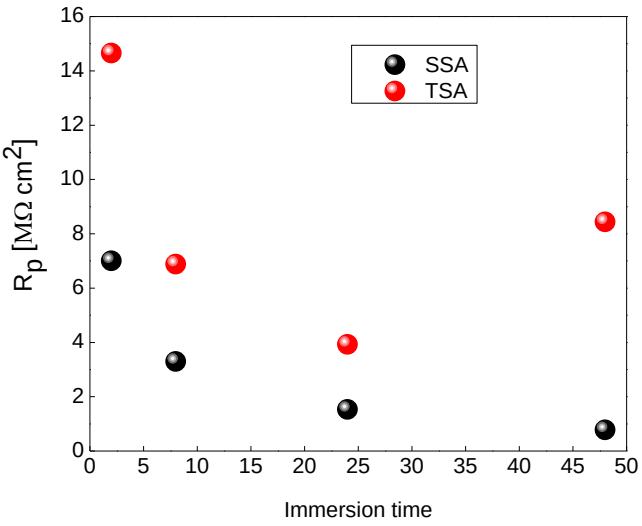

Figure 9. R_p Variation as a function of immersion time for anodic layers TiO_2 formed by SSA and TSA

However, for the TSA sample, noticeable high R_p values 14.66 MΩ.cm^2 were achieved at the beginning of immersion. Then, a slight decrease to 3.91 MΩ.cm^2 followed by a sharp increase to 8.50 MΩ.cm^2. This trend may be explained by a slight dissolution of the anodic film in the first stage. The anodic film was then shown to be more resistant to dissolution in a corrosive solution due to its more compact structure in this case. Thus, a less porous surface improves corrosion performance by restricting the entrance of chloride to the passive film.

On the other hand, the oxide film thickness played a major role in reducing the susceptibility of the specimen to corrosion. Anodization does not alter the substrate's corrosion mechanism, but it does reduce corrosion activities [32]. Similar trends in the anodic layer have been reported in recent studies by J. Winiarski et al. [16]. With a titania anodic film treated at 30 V in a choline dihydrogen citrate salt of oxalic acid. R. M. Bandeira et al. discovered a comparable value (14.3 MΩ.cm^2) after 24 hours of exposure in solution rings of Ti-6Al-4V anodic film treated with 80 V alternating current in an aqueous oxalic acid dihydrate solution.

3.6.2. Dynamic potential polarization

Polarization curves for the anodized samples are shown in Figure 10. Current density (i_{corr}) and corrosion potential (E_{corr}) were calculated from the Tafel curve by extrapolating the linear portion of the curves. Polarization resistance (R_p) is calculated from the equation [34]:

$$R_P = \frac{\beta_a \beta_c}{2.03\, i_{corr}(\beta_a + \beta_c)} \qquad (2)$$

where β_a and β_c are the tafel's anodic and cathodic slopes, respectively, and R_p is the polarization resistance.

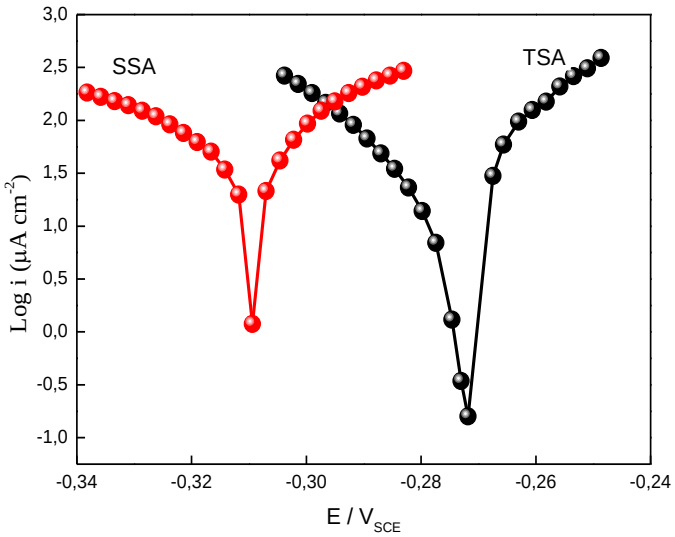

Figure 10. Potentiodynamic polarization curves of the TiO_2 anodic layers in 3.5 wt.% NaCl solution at 25 °C for 1 h

Table 1. Corrosion parameters of the TiO_2 anodic layers formed by SSA and TSA

	E_{corr} (V)	R_p (MΩ. cm^2)	i_{corr} (µA.cm^{-2})	β_c	β_a
SSA	-0.309	07.60	1.410	51.35	|-38.375|
TSA	-0.271	14.95	1.032	112.61	|-43.39|

A summary of the fitting results is given in Table 1. From the results illustrated in Table 1, the corrosion potentials of the TSA anodized specimen (-0.271 V/SCE), are higher than those of the SSA (about -0.309 V/SCE). Meanwhile, there is a considerable decrease in the corrosion current density of the TSA anodized specimen 1.032 (µA.cm^{-2}); it was significantly lower than (i_{corr}) of the SSA sample 1.410 (µA.cm^{-2}). In agreement with the EIS results, a noticeable high R_p value (14.95 MΩ.cm^2) was obtained after 1 hour of immersion time of the

specimen in NaCl solution; this value is approximately twice that obtained by SSA (07.60 $M\Omega.cm^2$).

The corrosion protection efficiency of the anodic coatings is evident from both the increase in corrosion potential and the reduction in corrosion current density. There was an enhancement of corrosion resistance by the TSA approach with the higher (E_{corr}) and lower (i_{corr}) values. This finding might be related to the fact that the thicker oxide film acts as a protective barrier, showing better corrosion resistance. Since the oxide film thickness played a major role in reducing the susceptibility of the specimen to corrosion, this can also be explained by the highly dense, uniform, and more compact continued adherent titania layer on the metal surface, which prevents chloride from entering the passive film.

In contracts, the SSA sample has a heterogeneous distribution of porosity and cracks on the surface of the anodic film, which allows Cl^- to easily penetrate the oxide film and affect its corrosion resistance. Also, recent research by Zhiwen Wang et al. [12] reported similar results. They have found that the two-step anodic oxidation enhanced the corrosion resistance of anodized titanium. The approximate value of the corrosion potential (-0.293 V/SCE) has been found by Weimin Jiang [35] for the sample treated by the second-step anodization in the fluoride-containing electrolyte at 20 V. In a recent study by Allal et al. [36], the optimization of operating factors influencing the titanium anodizing process has been realized for the properties of the TiO_2 layer, such as film thickness and polarization resistance. They found polarization corrosion around (5.08 $M.cm^{-2}$) with an anodic film thickness of 39 m anodized in H_2SO_4 (18% wt) at 60 V for 1 hour. In a recent study by Degnah et al. [3] on Ti-Zr-Fe-N-H system properties for marine applications, they discovered 1.5% Fe, -280 mV corrosion potential, and 0.46 $A.cm^{-2}$ corrosion current density. Gurrappa [6] discovered a corrosion potential of -436.9 mV and a corrosion current density of 58.46 $A.cm^{-2}$ in their study on the properties of titanium alloy Ti-6Al-4V for marine applications at 25 °C.

As a result, corrosion resistance has been enhanced by the TSA process; a more compact morphology represents a sealed structure that reduces the contact between the barrier layer and the outer layer, reducing corrosion propagation. The SEM morphology, thickness calculated by EDX, and GDOES analysis confirm the conclusions drawn from the experimental results of potentiodynamic polarization and EIS measurements.

4. CONCLUSION

A comparative study on the electrochemical behavior of TiO_2 anodic films formed by single-step (SSA) and two-step (TSA) anodizing processes has been investigated. The structural, morphological, and chemical composition of the films were presented and discussed. XRD diffraction confirmed the presence of the TiO_2 phase for SSA and TSA. EDS confirmed the formation of TiO_2 by the presence of titanium and oxygen on the surface of anodized films. The TSA process significantly improved corrosion resistance by forming a

highly dense, uniform, compact, and continuous adherent TiO_2 layer on the metal surface by reducing defects and channels available for Cl^- ion passage. Whereas the anodic film obtained by SSA is relatively porous and disorganized.

Acknowledgments

The authors are pleased to acknowledge the financial assistance of the "Department of Renewable Energy, and Chemical Engineering Laboratory, Department of Industrial Chemistry, Blida 1 University, Algeria" through the project.

Declarations of interest

The authors declare that they have no potential conflict of interest in relation to the study in this paper.

REFERENCES

[1] F.S. Ahmed, M.A. El Zomor, M.S. Abo Ghazala, and R.N. Elshaer, Sci. Rep. 12 (2022) 19265.

[2] M. Fazel, H.R. Salimijazi, M.A. Golozar, and M.R. Garsivaz jazi, Appl. Surf. Sci. 324 (2015) 751.

[3] A. Degnah, H.F. Alnaser, E.M. Sherif, I. Alhoweml, K.K. ondoh, and A. Alhazaa. Mater. Today Commun. 32 (2022) 103978.

[4] I.V. Gorynin, A.S. Oryshchenko, V.P. Leonov, V.I. Mikhailov, and I.A. Schastlivaia, Titanium application in marine engineering and nuclear-power engineering. Proceedings of the 13th World Conference on Titanium. San-Diego, USA (2015) pp. 302.

[5] X. Xu, P. Guo, X. Zuo, L. Sun, X. Li, K.R. Lee, and W. Aiying, Sur. Coat. Technol. 402 (2020) 1263472.

[6] I. Gurrappa, Mater. Charact. 51 (2003) 131**.**

[7] L. Wu, J. Liu, M. Yu, S. Li, H. Liang, and M. Zhu, Int. J. Electrochem. Sci. 9 (2014) 5012.

[8] W. Zhiwen, R. Ju, Z. Yannan, Y. Xiaohua, and Z. Zhaolin, Int. J. Electrochem. Sci. 13 (2018) 9681.

[9] Z. Liu, X. Liu, U. Donatus, G.E. Thompson, and P. Skeldon, Int. J. Electrochem. Sci. 9 (2014) 3558.

[10] L. Bouchama, N. Azzouz, N. Boukmouche, J.P. Chopart, A.L. Daltin, and Y. Bouznit, Surf. Coat. Technol. 235 (2013) 676.

[11] X. Yu, Y. Li, W. Ge, Q. Yang, N. Zhu, and K. Kalantar-zadeh, Nanotechnol. 17 (2006) 808.

[12] Z. Wang, J. Rong, Y. Zhang, X. Yu, and Z. Zhan, Int. J. Electrochem. Sci. 13 (2018) 9681.
[13] A.S.D. Al-Radha, Int. J. Sci. Res. 6 (2017) 2000.
[14] S.K. Lazarouk, D.A. Sasinovich, O.V. Kupreeva, T.I. Orehovskaia, N. Rochdi, F. Arnaud d'Avitaya, and V.E. Borisenko, Thin Solid Films 526 (2012) 41.
[15] L.T. Fuhr, Â.B.D. Moura, C.L.P. Carone, F.D.P. Morisso, L.F. Scheffel, S.R. Kunst, J.Z. Ferreira, and C.T. Oliveira, Revista Matéria. 25 (2020).
[16] J. Winiarski, A. Niciejewska, M. Górnik, J. Jakubowski, W. Tylus, and B. Szczygieł, RSC Adv. 11 (2021) 21104.
[17] S.A. Fadl-allah, and Q. Mohsen, Appl. Surf. Sci. 256 (2010) 5849
[18] M.R. Garsivaz jazi, M.A. Golozar, K. Raeissi, and M. Fazel, J. Mater. Eng. Perform. 23 (2014) 1270.
[19] I. Milosev, T. Kosec, and H.H. Strehblow, Electrochim. Acta 53 (2008) 3547.
[20] H.Y. Zheng, H.X. Qian, and W. Zhou, Appl. Surf. Sci. 254 (2008) 2174.
[21] Z. Liu, and G.E. Thompson, J. Mater. Eng. Perform. 24 (2015) 59.
[22] M. Prida, E. Manova, V. Vega, M. Hernandez-Velezb, P. Aranda, K.R. Pirota, M. Vázquez, and E. Ruiz-Hitzky, J. Magn. Magn. Mater. 316 (2007) 110.
[23] H.Z. Abdullah, M.A. Selimin, M.I. Idris, N. Anjang, and Z. Malik, Effect of sulphuric acid concentration on anodised titanium for biomedical application. Third International Conference on Advances in Civil, Structural and Mechanical Engineering-CSM, Institute of Research Engineers and Doctors, USA (2015).
[24] K. Indira, S. Ningshen, U. Kamachi Mudali, and N. Rajendran, in Thin Film and Nanomaterials, ed by S. Jayakumar, M. D. Kannan, R. Balasundaraprabhu and S. Prassana, Effect of anodization temperature on the surface morphology of anodized titanium (2011).
[25] R.G. Toro, M. Diab, T. de Caro, M. Al-Shemy, A. Adel, and D. Caschera, Materials 13 (2020) 1326.
[26] S.C. Vanithakumari, R.P. George, and U. Kamachi Mudali, Appl. Surf. Sci. 292(2014) 650.
[27] J. Liu, J. Yi, S. Li, M. Yu, G. Wu, and L. Wu, J. Appl. Electrochem. 40 (2010) 1545.
[28] J. Liu, L. Wu, M. Yu, S. Li, G. Wu, and Y. Zhang, J. Wuhan Univ. Technol. Mater. Sci. Ed 31 (2016) 599.
[29] B. Bozzini, P. Carlino, L. Durzo, V. Pepe, C. Mele, and F. Venturo, J. Mater. Sci. Mater. Med. 19 (2008) 3443.
[30] N. Bayat, S. Sanjabi, and Z.H. Barber, Appl. Surf. Sci. 257 (2011) 8493.
[31] E. Liu, and H.W. Kwek, Thin Solid Films 516 (2008) 5201.
[32] A.M. Habieb, and A. Anawati, Int. J. Corros. Scale Inhib. 11 (2022) 266.

[33] R.M. Bandeira, G.C. Rêgo, C.A. Picone, J.V. Drunen, W.R. Correr, L.C. Casteletti, S.A.S. Machado, and G. Tremiliosi-Filho, SN Appl. Sci. 2 (2020) 1092.
[34] D. Osorio, J. Lopez, H. Tiznado, M.H. Farias, M.A. Hernandez-Landaverde, M. Ramirez-Cardona, J.M. Yañez-Limon, J.O. Gutierrez, J.C. Caicedo, and G. Zambrano, Crystals 10 (2020) 620.
[35] W. Jiang, H. Cui, and Y. Song, J. Mater. Sci. 53 (2018) 15130
[36] N. Allal, A. Bourahla, F. Benharcha, A. Abdi, Z. Bekkar Djeloul Sayah, and M. Trari, J. Indian Chem. Soc. 99 (2022) 100470.